Heat losses in water pit thermal energy storage systems in the presence of groundwater

Sifnaios, Ioannis; Jensen, Adam R.; Furbo, Simon; Fan, Jianhua

Published in:
Applied Thermal Engineering

Link to article, DOI:
10.1016/j.applthermaleng.2023.121382

Publication date:
2023

Document Version
Publisher's PDF, also known as Version of record

Applied Thermal Engineering 235 (2023) 121382

Contents lists available at ScienceDirect

Applied Thermal Engineering

journal homepage: www.elsevier.com/locate/apthermeng

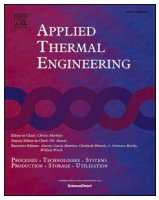

Research Paper

Heat losses in water pit thermal energy storage systems in the presence of groundwater

Ioannis Sifnaios [a,b,*], Adam R. Jensen [a], Simon Furbo [a], Jianhua Fan [a]

[a] Department of Civil and Mechanical Engineering, Technical University of Denmark, Koppels Allé 404, 2800, Kgs. Lyngby, Denmark
[b] Sino-Danish College (SDC), University of Chinese Academy of Sciences, Beijing, China

ARTICLE INFO

Keywords:
PTES
Heat storage
Computational Fluid Dynamics
CFD
Ground water

ABSTRACT

Water pit thermal energy storage (PTES) systems have proven a cheap and efficient storage solution for solar district heating systems. This is partly due to their low cost, deriving from low material usage as the ground is used as the weight-bearing structure. Further savings are obtained by the absence of insulation toward the ground, although this makes the ground-storage thermal interaction more pronounced than other storage technologies. However, it remains unclear how the different operation strategies affect the ground temperature and heat losses, especially in cases where groundwater is present. A simulation model was created using ANSYS and validated using operation data from the PTES in Marstal to investigate this. Using the validated model, it was found that the presence of groundwater could increase heat losses up to 60%, while the heat losses were unaffected when the groundwater table was more than 13 m below the storage bottom. The groundwater temperature could be maintained below 20 °C for a seasonal PTES if the groundwater table was at a depth of 25 m. However, maintaining this temperature for a short-term PTES operation was not feasible. Generally, the soil temperature was unaffected outside of a 100 m radius around the storage regardless of the operation type or the soil's thermal properties.

1. Introduction

Thermal energy storage (TES) systems have been used in connection with large-scale solar heating plants for district heating (DH), enabling DH systems to achieve solar fractions of up to 50% [1]. For seasonal storage, four main types of TES have been utilized, namely, pit thermal energy storage (PTES), borehole (BTES), aquifer (ATES), and tank (TTES) [2]. While TTES and PTES typically use water as a storage medium, BTES systems use the soil itself [3], and ATES use natural underground aquifers as the storage medium [4]. Classification of TES can also be based on installation; ATES, BTES, and PTES are all underground, while TTES are usually placed above ground. Nonetheless, in some cases, large-volume TTES can be placed partially underground (e.g., as in [5]).

Except for TTES, which are insulated against the ground, the other seasonal storage technologies are in direct contact with the soil. For example, the sides and bottom of PTES systems are uninsulated and only lined with a watertight polymer liner to prevent water from leaking into the ground [6]. Consequently, the soil's thermal properties directly affect the heat losses and performance of PTES.

Heat transfer in the soil is mainly driven by thermal conduction [7], although it should be noted that soil is a multi-phase material and can consist of solid, gas, and liquid particles. While the presence of gas (i.e., air) obstructs heat conduction, its replacement with liquid (i.e., water) increases the thermal conductivity of the soil [8]. Additionally, higher moisture content can increase the soil's specific and volumetric heat capacity [9]. In general, the effective thermal properties of soil depend on the soil type, mineralogy, particle size, packing geometry, porosity, degree of saturation, and the state of the water (i.e., liquid or solid) [10,11].

High soil thermal conductivity (e.g., water-saturated soils) has been shown to increase heat losses, negatively impact efficiency, and reduce the achievable temperature of seasonal heat storage systems [12]. Thus, from a heat loss perspective, it is evident that placing underground TES systems in locations with low soil thermal conductivity is beneficial.

Similarly, the presence of groundwater, especially flowing groundwater, has been found to affect the efficiency of TES systems negatively. For example, the efficiency of ATES can drop as low as 10% for cases with groundwater flow rates higher than 50 m/year [13]. Depending on the velocity of the groundwater flow, the efficiency of BTES systems can

* Corresponding author.
E-mail address: iosif@dtu.dk (I. Sifnaios).

https://doi.org/10.1016/j.applthermaleng.2023.121382
Received 1 June 2023; Received in revised form 14 July 2023; Accepted 14 August 2023
Available online 16 August 2023

be reduced by up to 30% [14]. Similarly, PTES systems can have approximately 15% higher heat loss due to groundwater [15]. Last, the efficiency of TTES systems can be reduced by 8% due to the presence of groundwater [16]. In general, it is acknowledged that the most favorable geological conditions for TES systems are when there is no groundwater [17,18] or with a low flow rate (e.g., groundwater flow rates less than 1 m/year are acceptable for BTES [19]). Nonetheless, there are cases where TES systems are located within the groundwater table due to the absence of local sites with favorable soil conditions or poor planning.

The TES-groundwater interaction leads to reduced TES performance but also to an increase in the groundwater temperature. Since approximately half of the world's population relies on groundwater for potable water supply [20], it is paramount to ensure that the water quality is not negatively affected by the change in groundwater temperature. Studies have shown that temperature can considerably alter the groundwater's chemical composition, and an increase of 5–10 K is generally acceptable [21]. As a rule of thumb, as temperature increases, there is an increase in the concentration of some bacteria and chemical elements (e.g., manganese), which can be harmful to humans [22].

For this reason, some European countries have placed limits on the maximum groundwater temperature, e.g., in Austria (20 °C), Denmark (25 °C), and the Netherlands (25 °C) [23]. Additionally, a relative change in the groundwater temperature of ±6 K is given in the geothermal installation guidelines in Austria (legally binding) and Germany (recommended) [23] and ± 3K in Switzerland (legally binding) [24].

To adhere to these regulations, Dahash et al. [16] investigated the impact of a groundwater barrier and the addition of insulation between the groundwater surface for PTES or the increase in the insulation thickness for TTES. They found that, for maintaining the groundwater temperature below 20 °C, a vertical water barrier (blocking groundwater movement around the storage) should be placed 25 m from the TES, combined with insulation around the TES. However, the study only investigated seasonal storage operation. In seasonal operation, PTES systems may act as the source for heat pumps; thus, the temperature operation range is usually 15 – 90 °C, while it is 45 – 90 °C for short-term operation. Due to the lack of research, it is unclear how the differences in long-term and short-term operations affect groundwater temperature. In addition, the study by Dahash et al. only considered a ten-year period, while the expected lifetime is 25 for a PTES and 40 years for a TTES. Thus, different results could be expected when simulating the full lifetime of the storage systems.

Besides the thermal conductivity of the soil domain and the presence of groundwater, the soil temperature can also affect the TES operation. The temperature of the upper soil layer fluctuates during the year mainly due to heat exchange with the ambient air, whereas an almost constant temperature is typically achieved at depths below 10 m [25]. However, heat losses from heat storage will gradually increase the temperature of the surrounding soil. Dahash et al. found that the ground temperature in the vicinity of a PTES or TTES can reach up to 50 °C during charging periods [26]. Moreover, simulations of a seasonal BTES system using the finite element simulation software COMSOL [27] indicated a 10 K temperature increase in the soil around the boreholes within one year and predicted a 16 K increase after five years [28]. In general, the ground heat losses of a TES can be divided into a periodic variation with an annual cycle and an initial part with a transient thermal build-up around the storage [29]. The transient temperature built-up around the storage is significant during the initial two to ten years of operation (depending on the storage size), while the periodic yearly variation is the most important long-term. Hence, it is important to investigate the heat loss of a TES system for several years as it is not constant, even if constant operation and ambient conditions can be assumed. However, it is not evident from the literature how long it takes for TES heat losses to stabilize due to the warm-up of the surrounding ground and if the length of this period depends on the operation (i.e., seasonal vs. short-term) and soil properties.

Traditionally, PTES had been used only for seasonal heat storage in conjunction with large-scale solar heating plants. However, in 2023, a new PTES was put into operation in Høje Taastrup (Denmark), which is operated as a short-term storage (two-week cycle) and is directly connected to the DH grid [30]. Thus, PTES can be used for both seasonal and short-term operations, unlike other storage technologies (e.g., ATES and BTES).

However, the change in operation strategy significantly alters the seasonality of the heat losses to the ground, although this has yet to be studied in detail. For this reason, the aim of this study is to elucidate the effect of different PTES operations on the surrounding ground and groundwater. Additionally, the effect of seasonal and short-term operations on groundwater will be investigated.

The present study focused on PTES, a promising heat storage technology combining low construction costs with high storage efficiency. The efficiency of the existing seasonal PTES varies from 60% to greater than 90% [31]. However, there are no specific guidelines regarding the optimal ground conditions for a PTES, and it is currently unclear how large of an impact ground conditions have on PTES performance. For example, at the Dronninglund PTES, there is a groundwater Table 1–1.5 m below the storage bottom with a flow rate of 15 m/year [32]. For maintaining a lower construction cost than TTES, PTES systems are not insulated toward the ground. Thus, they are expected to be influenced by the ground conditions much more than insulated technologies (e.g., TTES). Nevertheless, it remains unknown if and how much the groundwater affects the PTES performance and if the storage operation increases the groundwater temperature.

For this reason, the present study aims to investigate the following research questions:

- How long does it take for the ground temperature around a PTES to stabilize under short- and long-term operation?
- How large is the temperature zone of influence for a PTES?
- At what depth does the groundwater need to be for it not to affect PTES performance?
- How far from the PTES should groundwater be to satisfy the groundwater temperature regulations?

To answer these questions, a simulation model of the soil surrounding a PTES was developed and used to study the heat losses from the water-ground interface and the temperature development in the soil domain. The model was validated by comparison against measurement data from the PTES in Marstal. The validated model was used to simulate heat losses to the ground assuming different soil conductivities and groundwater conditions for short-term and seasonal PTES operations.

The PTES in Marstal is described in Section 2.1, followed by the description of the developed simulation model in Section 2.2. Section 2.3 presents the PTES water temperature profiles, and Section 2.4 the groundwater settings used in the simulations. The validation of the simulation model is presented in Sections 3.1 and 3.2, followed by the investigations for heat loss stabilization in Section 3.3. The PTES interaction with the surrounding soil is presented in Section 3.4, followed by the interaction with groundwater in Section 3.5. Last, the conclusions are presented in Section 4.

2. Methods

2.1. The PTES in Marstal

The PTES system in Marstal was constructed in 2012 with an approximate storage capacity of 6,000 MWh. The storage had the shape of an inverse truncated pyramid, with a volume of 75,000 m^3. The storage depth was 16 m, and the floating lid measured 113 by 88 m. The PTES was charged with heat from a 15,000 m^2 flat-plate solar collector field and used primarily for seasonal storage. Hence, the PTES was mainly charged during spring and summer and discharged during

autumn and winter.

The DH supply temperature in Marstal was approx. 73 °C, while the average return temperature was 40 °C [33]. When the temperature in the top layers of the PTES was sufficiently high, the storage could supply heat directly to the grid. However, when the storage temperature was below the supply temperature, the storage acted as a heat source for a 1.5 MW_{th} heat pump that supplied heat to the DH network. During autumn and winter, the heat pump operation lowered the PTES temperature to 15–20 °C. A more detailed description of the design and operation of the Marstal PTES can be found in [31]. An aerial photo of the solar collector field and PTES in Marstal can be seen in Fig. 1.

It should be mentioned that the Marstal PTES was used for validating the developed model due to the extensive ground temperature measurements.

2.1.1. Measurement locations and uncertainty

The water temperature inside the storage was measured using two temperature sensor strings mounted in the center of the lid. Each string had 16 temperature sensors placed at 1 m intervals. The two temperature strings were located next to each other but offset vertically by 0.5 m; thus, the vertical temperature profile was measured every 0.5 m. The temperature sensors were Class A PT100, with an accuracy of ±0.15 K.

Additionally, to monitor the change in ground temperature, four temperature sensor strings were installed near the edges of the storage embankment. The ground temperature sensors were PT100, but since their class is unknown, their accuracy was estimated to be ±0.5 K. The locations of all the temperature sensors are illustrated in Fig. 2.

2.1.2. Soil domain

The soil properties and groundwater conditions were assessed before the storage construction. Specifically, soil samples were taken from ten boreholes at a depth of either 14 or 24 m, with a uniform spatial distribution. Both intact soil samples were taken, and field vane tests were performed. The report of the soil investigations stated that the soil conditions were "messy," with alternating deposits of sand and clay and varying groundwater levels [35]. The stratigraphy of the terrain can be found in.

In many cases, groundwater was found at two different levels in the same borehole. However, the groundwater levels were different at each borehole. This indicated that there were probably isolated groundwater pockets in the area. Consequently, the exact dimensions and depth of the groundwater are unknown. Additionally, groundwater levels tend to change throughout the year due to rainfall, snowmelt, and dry periods [36].

According to the literature, the mean annual soil surface temperature in Denmark is 8 °C, and while there is a small increase with increasing depth, the temperature is within 8–12 °C down to a depth of 250 m [37]. No measurements were made of the soil's thermal properties; thus, the properties used in the simulations were taken from the literature, as summarized in Table 1. It has to be noted that, due to the high uncertainty regarding the extent of groundwater, uniform thermal properties were assumed for the entire soil domain.

Fig. 1. Aerial photo of the Marstal PTES in 2013 [34].

2.2. Simulation model of the PTES in Marstal

Heat losses from a PTES consist of heat losses through the insulated lid and through the uninsulated side and bottom walls. Accounting for the heat losses through the insulation lid is relatively straightforward as the phenomena can reasonably be assumed as one-dimensional. The heat losses through the lid are generally uniform, with some thermal bridges at the connection points of the insulation blocks. The main parameters affecting the lid heat losses are the ambient temperature, the top water layer temperature, and the effective heat loss coefficient of the lid. On the other hand, accounting for the heat losses to the ground is much more complex due to the non-negligible heat capacity of the soil. Consequently, the transient nature of the heat losses to the ground has to be considered and requires modeling in 3D. Several other parameters also affect the ground heat losses, e.g., the temperature gradient within the PTES, the soil's thermal properties, and the presence of groundwater.

For this reason, a 3D model of the soil domain around the PTES was developed using the finite volume method (FVM) software ANSYS Fluent. Fluent uses a numerical approach to solve the governing equations of fluid flow, offering a range of capabilities for simulating laminar and turbulent flows, heat transfer, etc. [39]. The simulation is conducted on a user-defined domain that is discretized using a computational mesh. Since this investigation focused on the heat losses toward the ground, the water and lid of the PTES were not explicitly modeled. By not modeling the movement of the water inside the PTES, only heat conduction in the soil had to be simulated instead of a fluid dynamics study, drastically reducing the computation time.

The heat losses from the water to the soil were simulated by applying the water temperature (varying with height) as a boundary condition on the soil's surface. This simplification was based on the following assumptions:

- The water temperature in the PTES can reasonably be described by 16 uniform-temperature layers, each 1 m tall.
- The convection coefficient between the water-soil interface is negligible relative to the thermal conduction in the soil.
- The water temperature profile is predominantly affected by charging/discharging and not by heat losses to the ground.

In the simulations, the soil domain was initialized with a uniform temperature of 8 °C. Heat exchange between the soil surface and the ambient air was simulated by applying a convection coefficient of 30 W/(m^2 K) to the exposed ground surface (corresponding to an average airflow velocity of 5 m/s) [40]. It has to be noted that the simulation of the soil domain did not account for solar radiation. In the first simulated year, corresponding to the construction period, the PTES soil was only exposed to the ambient temperature (pre-heating period) in order to achieve a realistic ground temperature profile to develop.

The extent of the surrounding soil domain had to be large enough to avoid the boundary conditions influencing the PTES operation. For this reason, the soil domain was extended 150 m away from the PTES edges, and the model had a depth of 200 m (see Fig. 3). Adiabatic boundary conditions were used for the side and bottom of the soil domain. In reality, there is some small heat gain from the Earth's core, but it was assumed negligible.

The created mesh consisted of hexahedral elements. The cells closer to the water-soil boundary have a higher density and a smaller size. This was done to ensure a high mesh density close to the heat source where large temperature gradients are expected. A mesh and timestep independence investigation was performed to confirm that the mesh was of sufficient quality and that an appropriate timestep had been selected

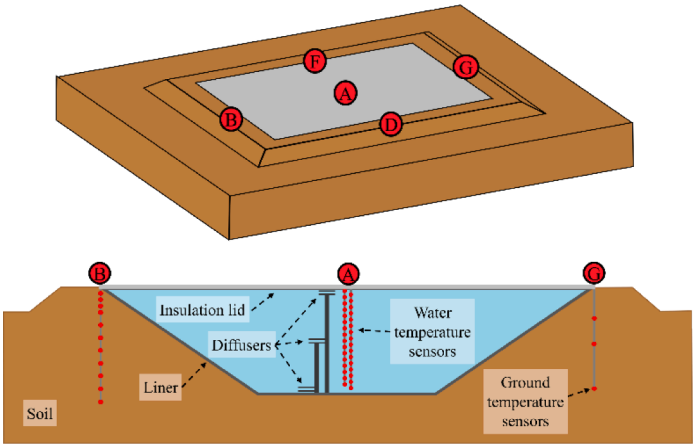

Fig. 2. Measurement sensor locations in the Marstal PTES. The water temperature strings are attached at location A, and the soil temperature is measured at locations B, D, F, and G. Each small red dot corresponds to a temperature sensor. (For interpretation of the references to color in this figure legend, the reader is referred to the web version of this article.)

Table 1
Thermal properties of sand and clay for different water contents (up to 25% for sand and 50% for clay) [38].

Soil type	Thermal conductivity [W/(m K)]	Specific heat capacity [J/(kg K)]	Bulk density [kg/m^3]
Sand (dry-moist)	0.3 – 1.9	590 – 1158	1800 – 2200
Sand (saturated)	2.0 – 3.0	956 – 1474	1900 – 2300
Clay (dry-moist)	0.4 – 1.0	789 – 842	1800 – 2000
Clay (saturated)	1.1 – 3.1	952 – 1333	2000 – 2200

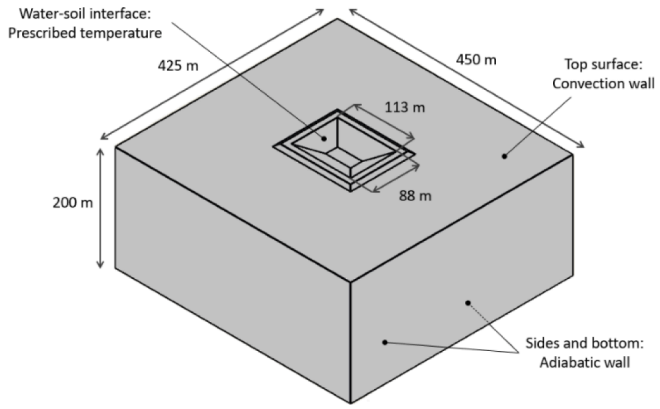

Fig. 3. The simulated soil domain and boundary conditions.

(see Section 3.1). Different mesh densities and timestep durations were selected and compared based on the calculated heat losses to the ground.

The model was validated by comparison against measured ground temperature data from the Marstal PTES from 2013 to 2016 (see Section 3.2).

2.3. Water temperature profiles

Theoretical temperature profiles were made corresponding to seasonal and short-term PTES operations. The seasonal PTES operation performed one charge–discharge cycle per year, with a temperature range of 90 – 15 °C (based on the actual operation of the PTES in Marstal [31]). The short-term operation was modeled as performing one charge–discharge cycle every two weeks (26 cycles per year), and the temperature range of the short-term operation was between 90 and 45 °C. The operation of the short-term PTES resembled the PTES in Høje Taastrup, Denmark [30,41]. It should be noted that for both storage operations, the top water layer was assumed to be constantly at 90 °C. The ambient temperature profile was taken from Denmark's Design Reference Year (DRY) [42]. Fig. 4 illustrates the mean storage temperature for the seasonal and short-term operations and the daily mean ambient temperature used in the simulations. The simulation duration was 25 years, so these profiles were repeated 25 consecutive times.

2.4. Groundwater simulation

For the initial investigations, the soil domain thermal properties were considered uniform and without the presence of groundwater. However, to investigate the interaction between the PTES and the groundwater, a groundwater layer was added to the domain for the simulations presented in Section 3.5. Realistic groundwater characteristics were taken from the PTES in Dronninglund [32] (presented in Table 2), as there was no pronounced groundwater layer at Marstal. This assumption was considered acceptable since similar geological

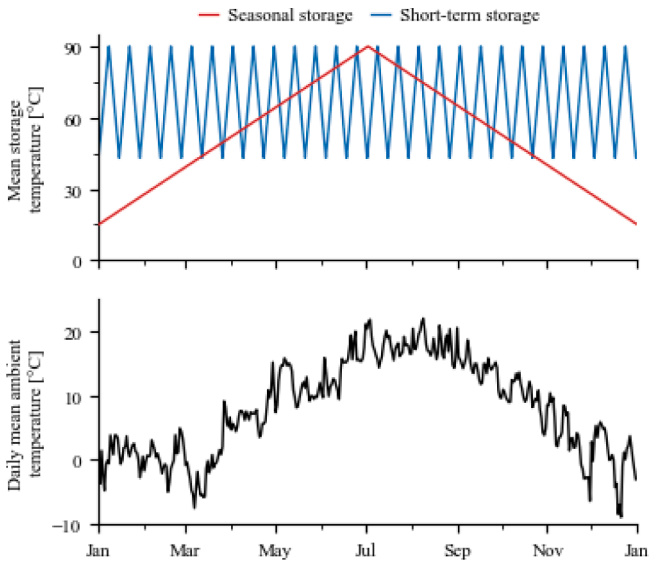

Fig. 4. Mean storage and ambient temperature for the simulated storage operations. The same conditions were repeated for each year of the simulation.

Table 2
Groundwater properties [44].

Parameter	Value	Unit
Hydraulic conductivity	$3.6 \cdot 10^{-5}$	m/s
Effective porosity	0.25	–
Hydraulic gradient	1/300	–
Groundwater velocity	$4.8 \cdot 10^{-7}$	m/s

conditions exist in Marstal and Dronninglund (i.e., the soil consists primarily of clay and sand). The groundwater was simulated as a 10 m layer, which is a representative value for confined aquifers [43] (and was also used in [16]) and was assumed to have the same temperature as the initial soil domain (i.e., 8 °C). However, it should be noted that groundwater characteristics can be very different depending on the investigated location.

The groundwater layer was simulated in ANSYS as a porous medium, and the flow was described using Darcy's law, as shown in Eqs. (1) and (2). Darcy's equations assume that the flow is laminar, viscous, and ignores convective acceleration and diffusion.

$$q = -\frac{\kappa}{\mu}\Delta p \tag{1}$$

$$u = \frac{q}{\varphi} \tag{2}$$

where q is the flux discharge per unit area, Δp is the pressure gradient vector, κ is the permeability, μ is the dynamic fluid viscosity, u is the fluid velocity, and φ is the porosity [45].

3. Results

3.1. Mesh and timestep independence of the CFD model

First, the mesh independence study was performed, where the heat losses for one year of operation were calculated for models with different numbers of cells. The calculated heat losses and the corresponding simulation time for each model are presented in Fig. 5. It can be observed that as the number of cells increased, the calculated heat loss for the scenarios with cells above 900 k reached an almost constant value, thus independent of the density of the mesh. The calculated heat loss for the scenario with 900 k cells differed only by 1% compared to the 3600 k case, while the simulation time was reduced by 73%. For this reason, it was decided that a mesh having 900 k cells was a good compromise between accuracy and simulation time. The mesh independence study was done using an 8 h timestep.

Next, the timestep independence was investigated using the mesh with 900 k cells. Similarly to the mesh independence, the calculated heat loss and simulation time for a simulation of one year of operation is presented in Fig. 5. The calculated heat loss for the case with the 8 h timestep differed by 0.7% compared to the 2 h case, while the simulation time was reduced by 68%. For this reason, a timestep of 8 h was chosen.

3.2. Model validation

The simulation model was validated against measured ground temperature data from the Marstal PTES for 2013 – 2015. As described in Section 2.2, the year 2012 was used as a pre-heating period.

In Fig. 6, measured ground temperatures can be observed at various depths. Depending on the level, each depth has two or four temperature sensors (see Fig. 2 and Section 2.1.1). The variation in the measured temperatures at the same depth demonstrates the mixed soil conditions around the PTES. In some cases, the temperature measured from two different sensors at the same height differed by up to 10 K, indicating the possible presence of groundwater pockets.

Comparing the simulated and measured temperatures in Fig. 6, it may be observed that the simulated ground temperatures follow the same trend as the measured ones at all depths, with an RMSE ranging from 0.22 to 1.54 K. Due to the highly uncertain ground conditions around the Marstal PTES (and also considering the sensor uncertainty), the difference between the simulated and measured temperatures was considered satisfactory. The following ground thermal properties were used in the simulation: thermal conductivity of 1.6 W/(m K), specific heat capacity of 800 J/(kg K), and bulk density of 2000 kg/m^3. These values are in line with the literature (see Table 1).

3.3. Heat loss and ground temperature stabilization

Fig. 7 presents the yearly heat losses toward the ground for a seasonal and short-term PTES operation for a period of 25 years. It can be observed that the heat losses decrease during the entire operation period of the PTES, with the first years having the most dramatic decrease. The reason for the reduction of heat loss with time is that when the PTES starts operating, the soil temperature around it is much lower than the charged water temperature. Thus, high heat transfer occurs from the PTES water to the soil. As the PTES continues to operate, heat accumulates in the soil, and the soil temperature increases; thus, the heat loss toward the soil decreases. More specifically, for the seasonal operation, the heat losses for the second year were 37% lower than the first.

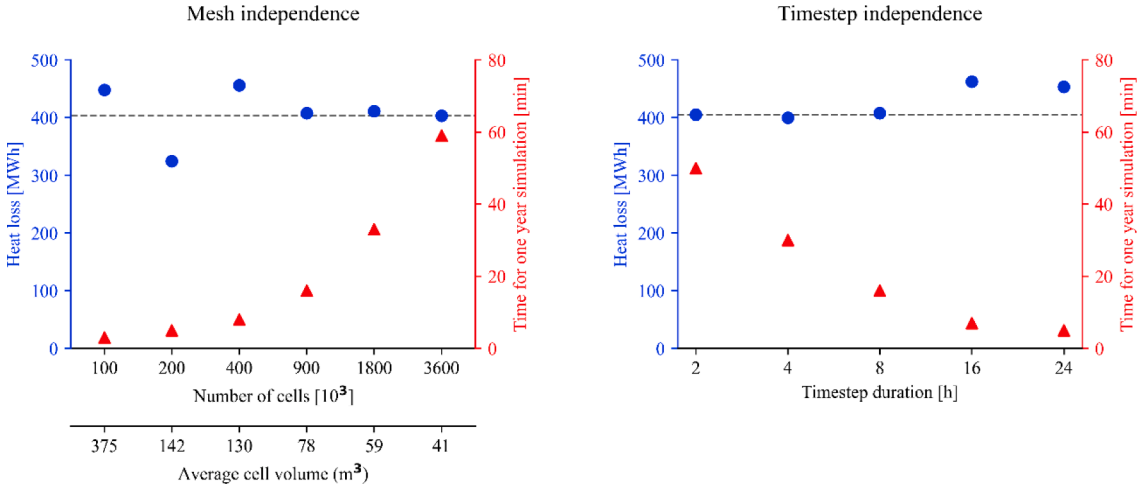

Fig. 5. Mesh (left) and timestep (right) independence results. The yearly heat loss is shown on the left y-axis (blue circles), and the time for one year of simulation is shown on the right y-axis (red triangles). (For interpretation of the references to color in this figure legend, the reader is referred to the web version of this article.)

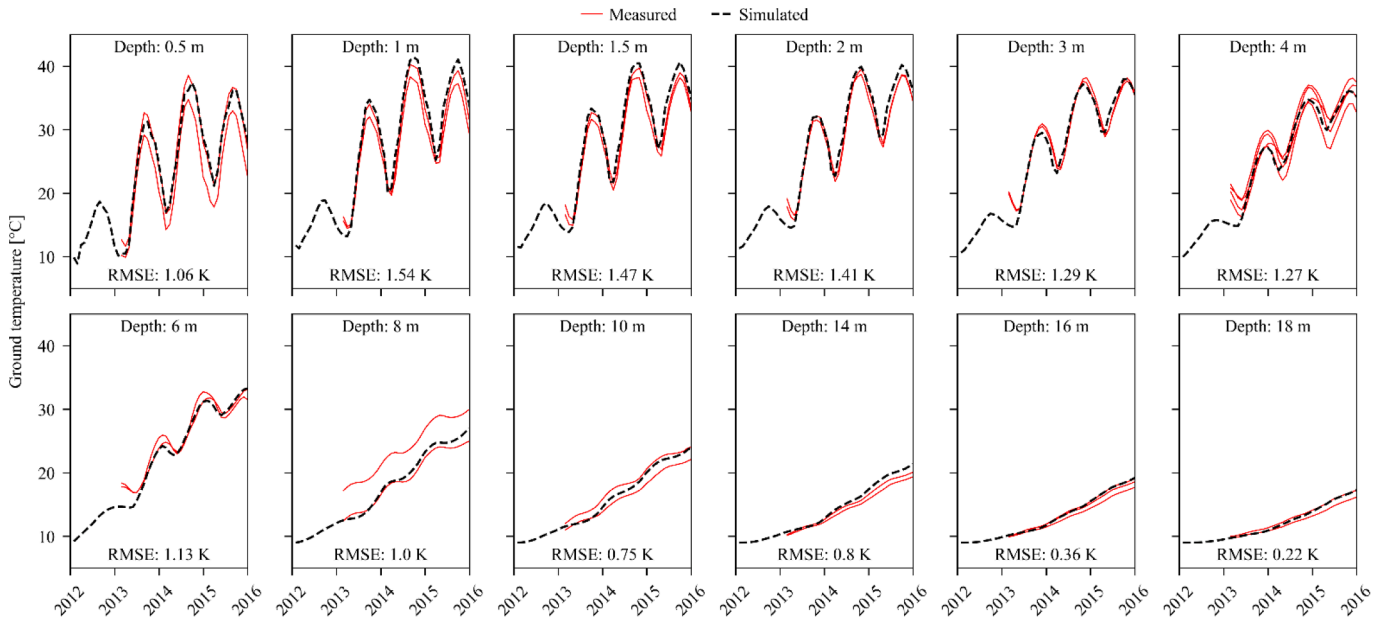

Fig. 6. Measured and simulated ground temperatures for the Marstal PTES from 2012 to 2015. Note that depending on the depth, there are two or four measured temperature curves.

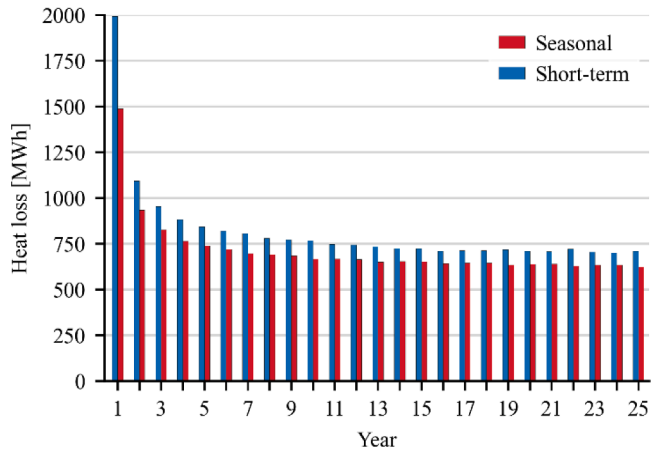

Fig. 7. Yearly heat losses toward the ground for seasonal and short-term PTES operation.

However, the third year was only 12% lower than the second. The heat losses in the last year of operation were 58% lower than the first. Although there was a decrease during the entire operation period (25 years), after the 12th year, the change in the heat losses from one year to the next was less than 2%, so the heat losses could be considered stable after this point.

A similar trend can be observed for the short-term PTES operation. For example, the second year of operation had 45% lower heat losses than the first, while the last year had 64% lower heat losses than the first. Overall, the heat losses stabilized quicker than the seasonal operation, i.e., in the 8th year of operation. It should also be noted that the short-term PTES had approximately 15% higher heat losses than the seasonal one due to the higher average water temperature. However, the relative heat losses of the short-term storage are lower than the seasonal, and thus the short-term efficiency is higher, although the annual heat losses are higher. This is due to the greater number of storage cycles of the short-term PTES, i.e., 10 – 20 times as much energy is stored annually.

The ground temperatures around the PTES for the 25 years of operation are presented in Fig. 8. It can be observed that, for both PTES operations, there is a yearly variation in the soil temperature close to the surface induced by the ambient temperature variation during the year. However, this variation is much more intense in the case of seasonal PTES operation. The reason is that a seasonal storage is discharged to much lower temperatures than a short-term (due to the heat pump operation). Thus, the soil temperature around the seasonal PTES is much lower in the winter (when it is empty) than the short-term PTES.

Fig. 8 also demonstrates that the soil temperature close to the PTES is not stabilized even after 25 years of operation (especially in lower depths). The increase in the soil temperature, even after 25 years of operation for the short-term PTES, is due to the higher minimum

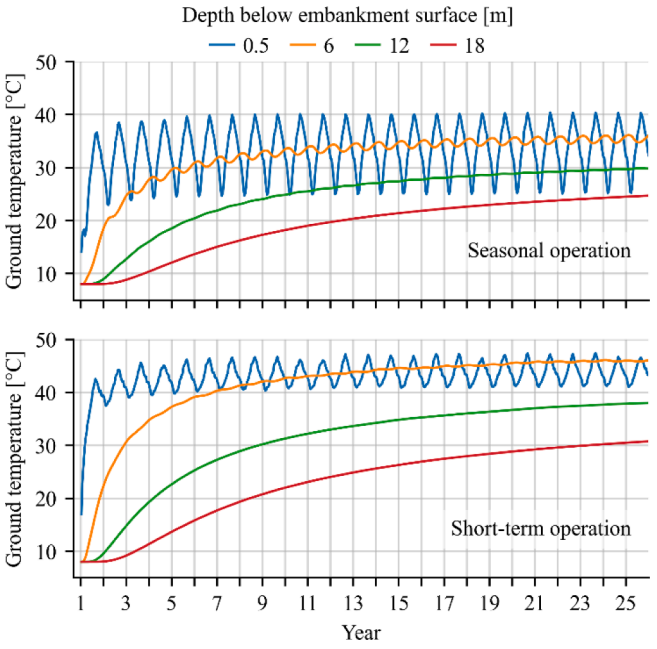

Fig. 8. Ground temperature development at different depths for seasonal and short-term PTES operations. The horizontal location corresponds to location B in Fig. 2.

temperatures of the short-term PTES compared to the seasonal. It is thus important to consider the entire lifetime of a PTES when assessing its effect on the surrounding soil and groundwater temperatures.

3.4. PTES zone of influence

In order to determine the dimensions of the soil domain that was affected by the operation of a PTES, a zone of influence was established. This zone was determined by calculating the soil temperature on a horizontal and a vertical line, starting at the bottom of the PTES and extending to the end of the soil domain (see Fig. 9).

A low and a high soil conductivity scenario were investigated to investigate the possible effect of soil conductivity on the size of the zone of influence. For the high conductivity scenario, a thermal conductivity of 3 W/(m K), a specific heat capacity of 1400 J/(kg K), and a bulk density of 2300 kg/m^3 was used. In contrast, for the low conductivity scenario, a thermal conductivity of 0.3 W/(m K), a specific heat capacity of 700 J/(kg K), and a bulk density of 1800 kg/m^3 was used. These values were the extremes for each parameter from Table 1. The ground temperatures are illustrated in Fig. 9 for both scenarios. It should be noted that Fig. 9 shows the temperature in the soil domain at the start of July (i.e., both storage types were fully charged) after 25 years of PTES operation.

As expected, the ground around the short-term PTES reached higher temperatures than the seasonal PTES. Additionally, the high-conductivity soil domain reached higher temperatures than the low-conductivity domain at the same depth. Nonetheless, the soil temperature was unaffected outside of a 100 m radius from the storage, regardless of the operation type or the thermal properties of the soil.

3.5. PTES and groundwater

The effect of groundwater on the soil temperature is illustrated in Fig. 10 after 25 years of PTES operation. In the previous sections of this paper, it was proven that the short-term operation of a PTES results in higher soil temperatures; thus, the results presented in Fig. 10 are only for short-term operation for space-saving purposes.

Fig. 10 presents calculated soil temperature contour plots for three

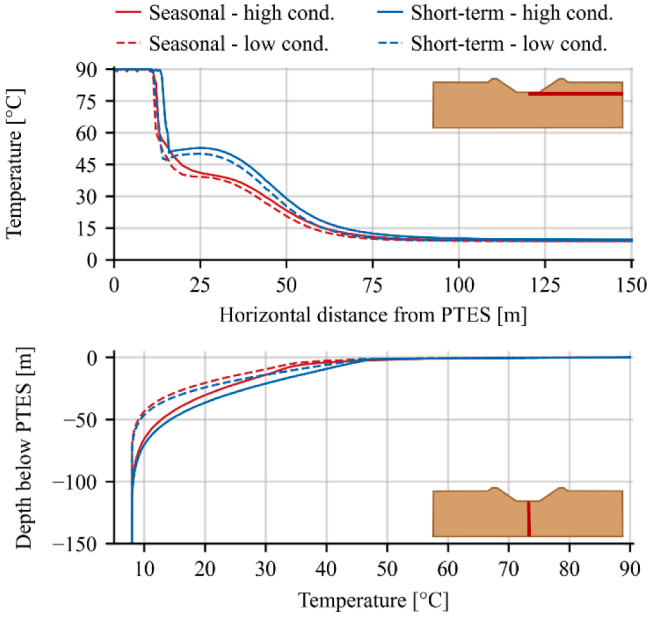

Fig. 9. Ground temperature profile after 25 years of operation for a high and low conductivity (cond.) soil domain. The soil temperature was calculated on a horizontal line and a vertical line. Both lines started at the bottom center of the PTES and extended to the end of the soil domain.

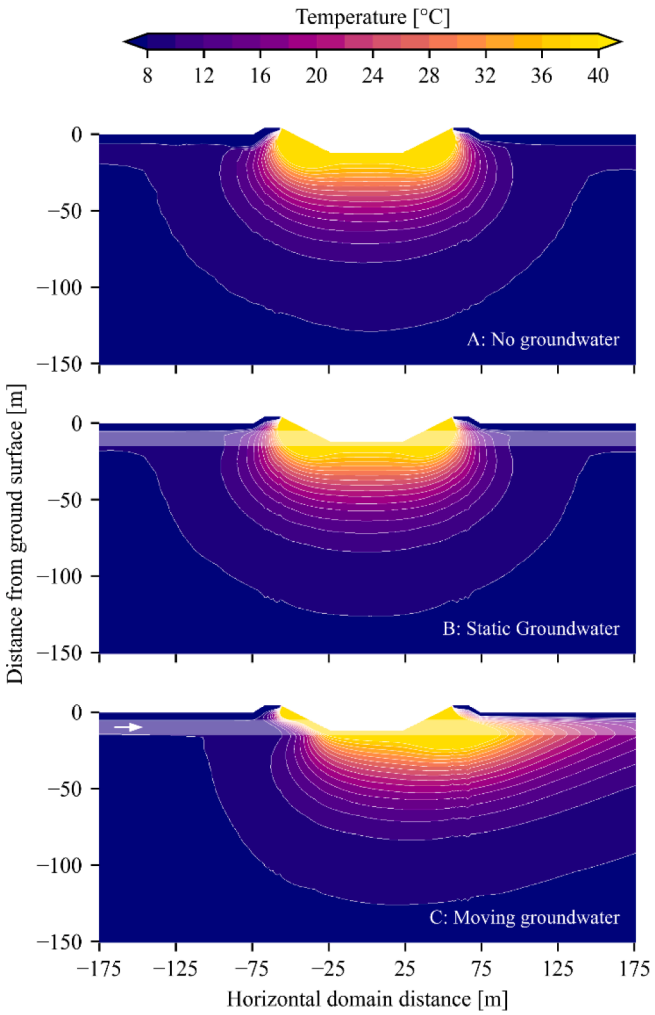

Fig. 10. Soil temperature contours for short-term PTES operation where there is no groundwater (A), one static groundwater layer (B), and one moving groundwater layer (C). The semi-transparent horizontal white bar in the bottom two subplots illustrates the groundwater layer.

groundwater scenarios; scenario (A) has no groundwater, (B) has a static groundwater layer, and (C) has a moving groundwater layer. The groundwater layer modeling was done as described in Section 2.4. The depth of the groundwater layer was 5 m below the ground surface (average depth for Denmark [46]), resulting in the bottom half of the PTES being within the groundwater layer.

It may be observed that the contours in (A) and (B) are very similar. However, in case (B), the soil temperatures are somewhat higher due to the presence of groundwater and, thus, higher thermal conductivity in this layer. As expected, the largest difference can be spotted in sub-figure (C), where, due to the moving groundwater, the temperature contours are shifted in the direction of the moving groundwater.

Apart from the differences in the soil temperature profiles, groundwater also impacted the heat losses. Table 3 presents each case's average yearly heat loss for the 25 years of operation for seasonal and short-term

Table 3
Yearly average heat losses toward the ground of the seasonal and short-term PTES operation for different groundwater conditions. Values are in MWh.

Scenario	Seasonal	Short-term
No groundwater	715	820
Static groundwater	820	927
Moving groundwater	1118	1333

PTES operations. It may be observed that both PTES operations are affected similarly, having approximately 14% higher heat losses for static groundwater (B) and approximately 60% higher heat losses for moving groundwater (C) compared to the case without groundwater (A).

It should be noted that the results in Table 3 are for a case where the groundwater is located 5 m below the ground surface (thus, the lower half of the PTES is surrounded by groundwater). Consequently, the next step was to investigate the impact of the depth of the groundwater layer. Since the highest heat losses occurred for the scenario with moving groundwater (15 m/year), this case was selected for investigating different depths. These results are presented in Fig. 11.

Fig. 11 presents the heat losses from a PTES operating in seasonal or short-term mode with different depths of the groundwater layer. As expected, the closer the groundwater layer is to the PTES bottom, the higher the heat loss. Specifically, the heat losses were approximately 40% higher when the groundwater was 5 m below the ground surface compared to when the groundwater layer was at 25 m.

It may be observed that the PTES heat losses were unaffected by the presence of groundwater at a depth of 25 m below the ground surface (or 13 m below the bottom of the PTES). This was true for both seasonal and short-term PTES operations.

Fig. 12 and Fig. 13 show the corresponding temperature profile for the seasonal and short-term PTES operation, respectively. The groundwater depth ranged from 5 m below the surface (A) to 30 m below the surface (F). It may be observed that the temperature contours are skewed toward the moving direction of the groundwater in both figures. In Fig. 12, the highest temperature contours (greater than 25 °C) are located only close to the PTES sides since the heat pump operation cools the bottom to lower temperatures. However, in Fig. 13, the highest temperature contour is located around all sides of the PTES. Generally,

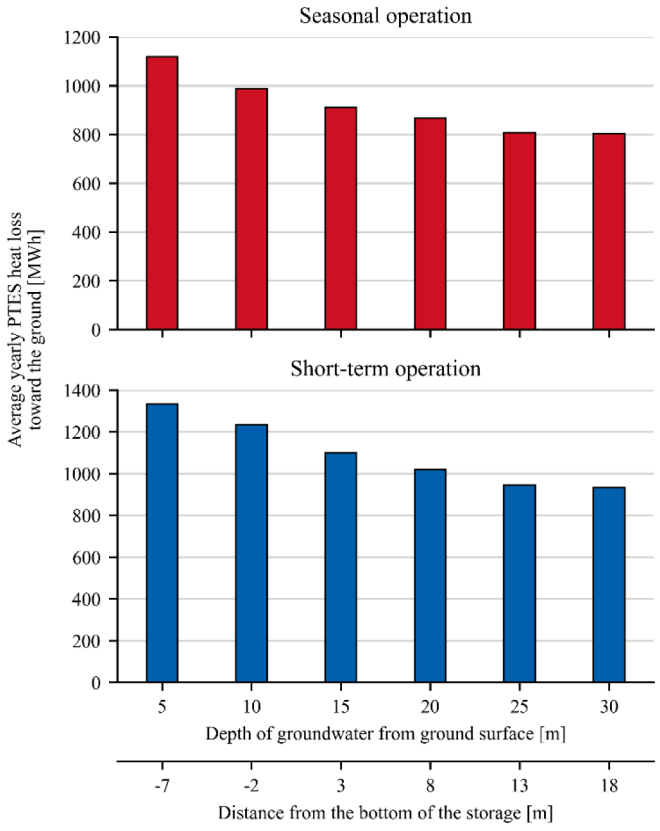

Fig. 11. Average yearly heat losses toward the ground for seasonal and short-term PTES operations at different groundwater depths for a moving groundwater layer.

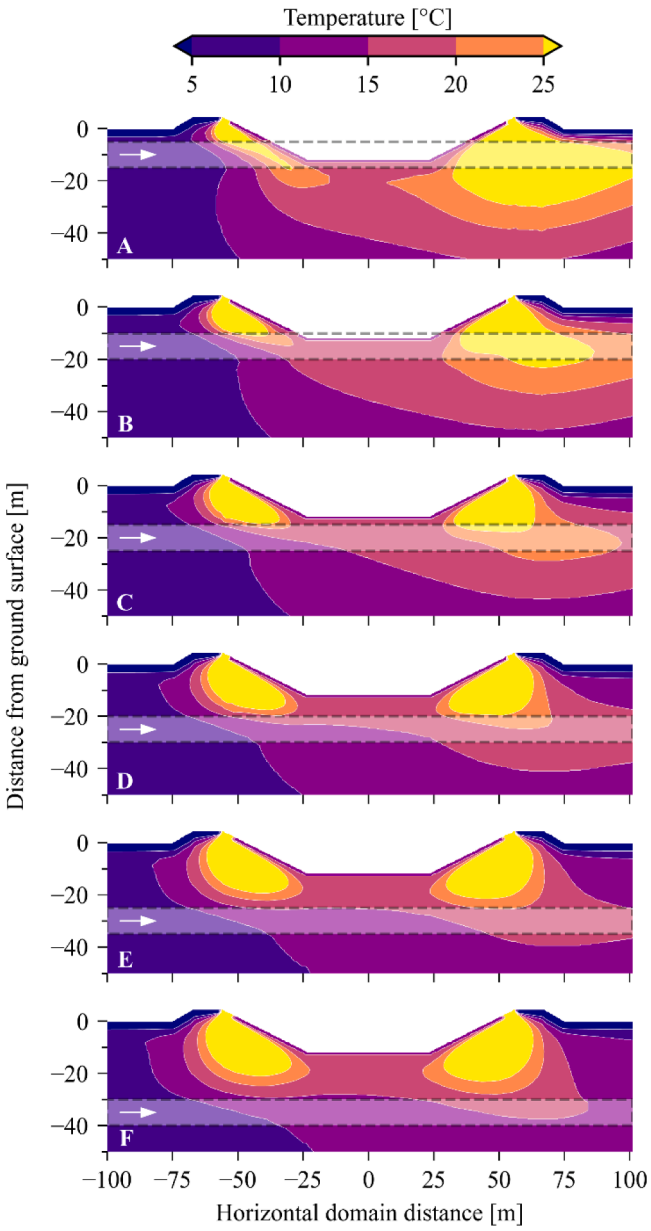

Fig. 12. Ground temperature contour plots for seasonal PTES operation for different depths of moving groundwater. The semi-transparent horizontal white bar illustrates the groundwater layer.

the soil temperature profile changes from the depth of the groundwater downwards.

According to the regulations mentioned in Section 1, the groundwater temperature should not exceed 20 – 25 °C (depending on the country). Thus, it can be observed that the temperature of the groundwater layer remains lower than 25 °C for depths below 20 m for the seasonal operation and below 30 m for short-term operation. In fact, the groundwater temperature was below 20 °C at a groundwater depth of 25 m for the seasonal operation, whereas it was not achievable for short-term operation.

Nevertheless, under no circumstances was it possible to limit the change of the groundwater temperature to ± 6 K, which is required in some countries. Thus, it can be concluded that, in countries where this is required, groundwater should not be present in the selected location. Alternatively, it may be advisable to increase the allowable heating of groundwater within a specified radius of heat storage systems and require documentation that local groundwater wells remain unaffected.

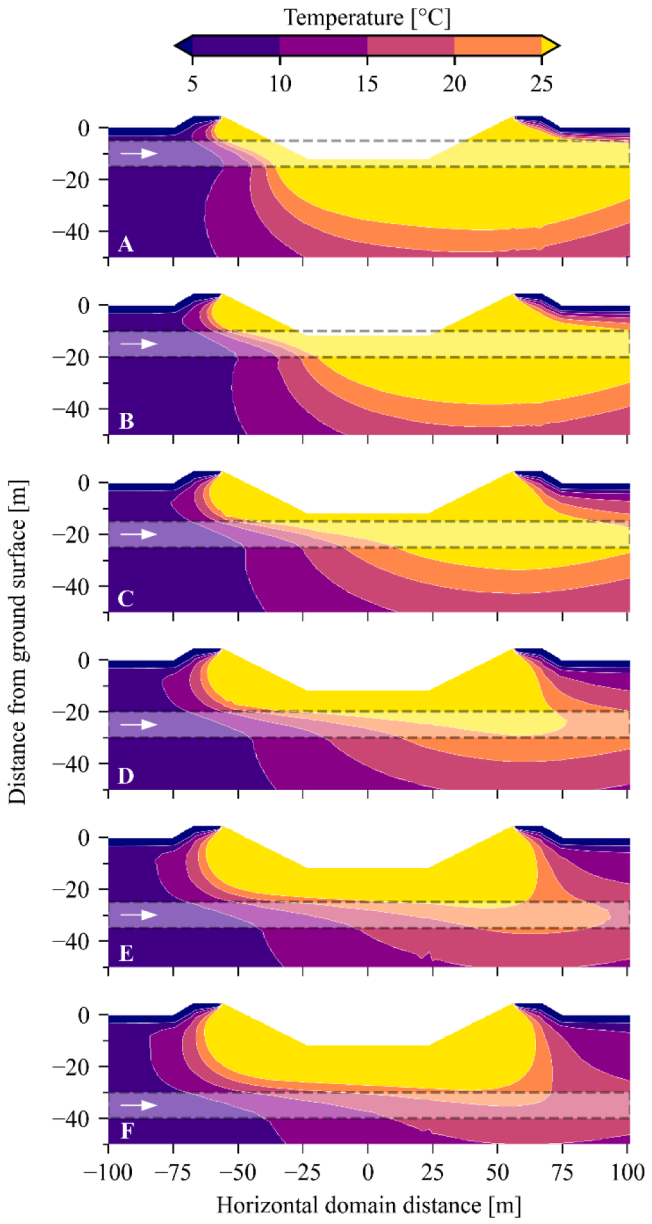

Fig. 13. Ground temperature contour plots for short-term PTES operation for different depths of moving groundwater. The semi-transparent horizontal white bar illustrates the groundwater layer.

4. Conclusions

This study investigated the effect of groundwater on PTES heat losses as well as the effect of PTES operation on the groundwater temperature. A simulation model was developed using ANSYS Fluent and was validated using operation data from the Marstal PTES. The model was modified to be able to simulate seasonal and short-term PTES operations and account for groundwater at different depths. The main conclusions from this study were the following:

- The soil temperature was unaffected at a 100 m radius around the PTES regardless of its operation or the soil's thermal properties.
- The heat losses of a short-term PTES stabilized after eight years of operation, while the heat losses of a seasonal PTES stabilized after 12 years.
- The short-term PTES had, on average, 15% higher heat losses than the seasonal PTES due to higher storage temperatures.
- Static groundwater increased the PTES heat losses by 14%, and for moving groundwater, the heat losses were increased by 60% compared to a case without groundwater.
- PTES heat losses were unaffected by the presence of groundwater when the groundwater table was 13 m below the bottom of the PTES.
- The groundwater layer could maintain a temperature lower than 25 °C at a depth of 20 m for seasonal PTES operation while at 30 m for short-term operation.
- The groundwater temperature was maintained below 20 °C for the seasonal operation at a groundwater depth of 25 m, whereas this was not possible for the short-term operation.

These conclusions can be used primarily in the planning stage of a PTES for choosing a construction location based on geological conditions. Accurate prediction of a storage performance is of major importance for securing financing and delivering the promised results to the DH system. Additionally, since environmental permits are required in most countries, it is important to be able to document that the PTES operation will not affect the groundwater or any cultivation in the vicinity.

Future work could include investigating different groundwater flow rates at different depths. Additionally, with the wider adoption of low-temperature district heating, it could be relevant to investigate different temperature operation ranges for seasonal and short-term operation. It is expected that with low-temperature district heating, the PTES heat losses would be lower, resulting in lower groundwater temperature.

CRediT authorship contribution statement

Ioannis Sifnaios: Conceptualization, Methodology, Visualization, Investigation, Writing – original draft. **Adam R. Jensen:** Methodology, Visualization, Writing – review & editing. **Simon Furbo:** Writing – review & editing, Supervision, Funding acquisition. **Jianhua Fan:** Supervision, Funding acquisition.

Declaration of Competing Interest

The authors declare that they have no known competing financial interests or personal relationships that could have appeared to influence the work reported in this paper.

Data availability

The authors do not have permission to share data.

Acknowledgments

This study was funded by the Danish Energy Agency through EUDP grant no. 64020-2036 (IEA Task 39: Large Thermal Energy Storages for District Heating) and by the Sino-Danish Center for Education and Research (SDC) Ph.D. program.

References

[1] D. Sveinbjörnsson, L. Laurberg Jensen, D. Trier, I. Ben Hassine, X. Jobard, Large Storage Systems for DHC, Networks (2017).
[2] T. Pauschinger, T. Schmidt, P. Alex Soerensen, D. Aart Snijders, R. Djebbar, R. Boulter, C. Jeff Thornton, Integrated Cost-effective Large-scale Thermal Energy Storage for Smart District Heating and Cooling - Design Aspects for Large-Scale Aquifer and Pit Thermal Energy Storage for District Heating and Cooling, Int. Energy Agency Technol. Collab. Program. Dist. Heat. Cool. Incl. Comb. Heat Power. (2018 (2018).).
[3] M. Reuss, The use of borehole thermal energy storage systems, in: L.F. Cabeza (Ed.), Adv. Therm. Energy Storage Syst. Methods Appl, 2nd ed., 2020, pp. 139–171, https://doi.org/10.1016/C2019-0-00061-1.
[4] L. Gao, J. Zhao, Q. An, X. Liu, Y. Du, Thermal performance of medium-to-high-temperature aquifer thermal energy storage systems, Appl. Therm. Eng. 146 (2019) 898–909, https://doi.org/10.1016/j.applthermaleng.2018.09.104.

[5] K. Narula, F.D.O. Filho, J. Chambers, M.K. Patel, Simulation and comparative assessment of heating systems with tank thermal energy storage – A Swiss case study, J. Energy Storage. 32 (2020), 101810, https://doi.org/10.1016/j.est.2020.101810.

[6] M.V. Jensen, Seasonal pit heat storages - Guidelines for materials & construction IEA-SHC Tech Sheet 45.B.3.2, 2014. http://task45.iea-shc.org/fact-sheets.

[7] A. Gabrielsson, U. Bergdahl, L. Moritz, Thermal energy storage in soils at temperatures reaching 90°c, J. Sol. Energy Eng. Trans. ASME. 122 (2000) 3–8, https://doi.org/10.1115/1.556272.

[8] Y. Dong, J.S. McCartney, N. Lu, Critical Review of Thermal Conductivity Models for Unsaturated Soils, Geotech. Geol. Eng. 33 (2015) 207–221, https://doi.org/10.1007/s10706-015-9843-2.

[9] N.H. Abu-Hamdeh, Thermal properties of soils as affected by density and water content, Biosyst. Eng. 86 (2003) 97–102, https://doi.org/10.1016/S1537-5110(03)00112-0.

[10] H.F. Zhang, X.S. Ge, H. Ye, D.S. Jiao, Heat conduction and heat storage characteristics of soils, Appl. Therm. Eng. 27 (2007) 369–373, https://doi.org/10.1016/j.applthermaleng.2006.07.024.

[11] N. Zhang, Z. Wang, Review of soil thermal conductivity and predictive models, Int. J. Therm. Sci. 117 (2017) 172–183, https://doi.org/10.1016/j.ijthermalsci.2017.03.013.

[12] G.J. van den Brink, C.J. Hoogendoorn, Ground water flow heat losses for seasonal heat storage in the soil, Sol. Energy 30 (1983) 367–371, https://doi.org/10.1016/0038-092X(83)90190-1.

[13] M. Bloemendal, N. Hartog, Analysis of the impact of storage conditions on the thermal recovery efficiency of low-temperature ATES systems, Geothermics 71 (2018) 306–319, https://doi.org/10.1016/j.geothermics.2017.10.009.

[14] H.J.G. Diersch, D. Bauer, Analysis, modeling, and simulation of underground thermal energy storage systems, LTD (2020), https://doi.org/10.1016/B978-0-12-819885-8.00007-3.

[15] A. Dahash, M. Bianchi Janetti, F. Ochs, Numerical Analysis and Evaluation of Large-Scale Hot Water Tanks and Pits in District Heating Systems, Build. Simul. Conf. Proc. (2019) 1692–1699, https://doi.org/10.26868/25222708.2019.210566.

[16] A. Dahash, F. Ochs, G. Giuliani, A. Tosatto, Understanding the Interaction between Groundwater and Large-Scale Underground Hot-Water Tanks and Pits, Sustain. Cities Soc. 71 (2021), 102928, https://doi.org/10.1016/j.scs.2021.102928.

[17] C. Suárez, J. Pino, F. Rosa, J. Guerra, Analytical approach to ground heat losses for high temperature thermal storage systems, Int. J. Energy Res. 43 (2019) 439–454, https://doi.org/10.1002/er.4278.

[18] K.S. Lee, Simulation on the cyclic operation of an open borehole thermal energy storage system under regional groundwater flow, Geosci. J. 14 (2010) 217–224, https://doi.org/10.1007/s12303-010-0020-6.

[19] T. Schmidt, T. Pauschinger, P.A. Sørensen, A. Snijders, R. Djebbar, R. Boulter, J. Thornton, Design Aspects for Large-scale Pit and Aquifer Thermal Energy Storage for District Heating and Cooling, Energy Procedia 149 (2018) 585–594, https://doi.org/10.1016/j.egypro.2018.08.223.

[20] World Water Assessment Programme, The United Nations World Water Development Report 3: Water in a Changing World., Paris: UNESCO, and London: Earthscan, 2009.

[21] C. Griebler, H. Brielmann, C.M. Haberer, S. Kaschuba, C. Kellermann, C. Stumpp, F. Hegler, D. Kuntz, S. Walker-Hertkorn, T. Lueders, Potential impacts of geothermal energy use and storage of heat on groundwater quality, biodiversity, and ecosystem processes, Environ. Earth Sci. 75 (2016), https://doi.org/10.1007/s12665-016-6207-z.

[22] T. Riedel, Temperature-associated changes in groundwater quality, J. Hydrol. 572 (2019) 206–212, https://doi.org/10.1016/j.jhydrol.2019.02.059.

[23] S. Haehnlein, P. Bayer, P. Blum, International legal status of the use of shallow geothermal energy, Renew. Sustain. Energy Rev. 14 (2010) 2611–2625, https://doi.org/10.1016/j.rser.2010.07.069.

[24] F. Stauffer, P. Bayer, P. Blum, N. Molina-Giraldo, W. Kinzelbach, Thermal use of shallow groundwater, Taylor & Francis Group, New York, 2014.

[25] C.O. Popiel, J. Wojtkowiak, B. Biernacka, Measurements of temperature distribution in ground, Exp. Therm Fluid Sci. 25 (2001) 301–309, https://doi.org/10.1016/S0894-1777(01)00078-4.

[26] A. Dahash, M.B. Janetti, F. Ochs, Detailed 3-D models of a large-scale underground thermal energy storage with consideration of groundwater conditions, in: Int. Sustain. Energy Conf., 2018: pp. 597–604.

[27] COMSOL, COMSOL Multiphysics software, (n.d.). https://www.comsol.com/ (accessed July 12, 2023).

[28] H.M.K.U. Haq, E. Hiltunen, An inquiry of ground heat storage: Analysis of experimental measurements and optimization of system's performance, Appl. Therm. Eng. 148 (2019) 10–21, https://doi.org/10.1016/j.applthermaleng.2018.11.029.

[29] G. Hellström Ground heat storage: Thermal analyses of duct storage systems 1991.

[30] VEKS, Høje Taastrup fjernvarme, Heat pit storage optimizes district heating, (2022). https://planenergi.eu/wp-content/uploads/2022/07/Heat-pit-storage_folder-2022_uk.pdf (accessed January 19, 2023).

[31] I. Sifnaios, A.R. Jensen, S. Furbo, J. Fan, Performance comparison of two water pit thermal energy storage (PTES) systems using energy, exergy, and stratification indicators, J. Energy Storage. 52 (2022), 104947, https://doi.org/10.1016/j.est.2022.104947.

[32] I. Sifnaios, G. Gauthier, D. Trier, J. Fan, A.R. Jensen, Dronninglund water pit thermal energy storage dataset, Sol. Energy 251 (2023) 68–76, https://doi.org/10.1016/j.solener.2022.12.046.

[33] Dansk Fjernvarme, Inspirations-katalog om solvarme, (2017). https://docplayer.dk/47760153-Solvarme-inspirationskatalog-inspirationskatalog-om-solvarme-inspiration-og-erfaringer-fra-solvarmeanlaeg-i-kombination-med-fjernvarme-i-danmark.html (accessed August 16, 2023).

[34] PlanEnergi, Design of the pit heat storage of the demonstration plant at Marstal Fjernvarme, 2013. https://docplayer.net/40878119-Sunstore-4-deliverable-d-2-2-version-3-design-of-the-pit-heat-storage-of-the-demonstration-plant-at-marstal-fjernvarme.html.

[35] GEO, Marstal damvarmelager geoteknisk undersøgelse, 2010.

[36] M. Nygren, M. Giese, B. Kløve, E. Haaf, P.M. Rossi, R. Barthel, Changes in seasonality of groundwater level fluctuations in a temperate-cold climate transition zone, J. Hydrol. X. 8 (2020), 100062, https://doi.org/10.1016/j.hydroa.2020.100062.

[37] I. Møller, N. Balling, C. Ditlefsen, Shallow subsurface thermal structure onshore Denmark: temperature, thermal conductivity and heat flow, (2018). https://2dgf.dk/xpdf/bull67-29-52.pdf (accessed July 13, 2023).

[38] Verein Deutscher Ingenieure (VDI), Thermische Nutzung des Untergrunds - Grundlagen, Genehmigungen, Umweltaspekte (2010). https://www.vdi.de/richtlinien/details/vdi-4640-blatt-1-thermische-nutzung-des-untergrunds-grundlagen-genehmigungen-umweltaspekte.

[39] ANSYS, ANSYS Fluent, (n.d.). https://www.ansys.com/products/fluids/ansys-fluent (accessed July 12, 2023).

[40] L. Laloui, A.F. Rotta Loria, Heat and mass transfers in the context of energy geostructures, in: Anal. Des. Energy Geostructures, Academic Press, 2020: pp. 69–135. 10.1016/b978-0-12-816223-1.00003-5.

[41] Høje Taastrup fjernvarme, Returtemperatur-tarif, (2022). https://www.htf.dk/returtemperatur-tarif (accessed February 27, 2023).

[42] Aalborg University, Climate Data, (n.d.). https://build.dk/bsim/Pages/Climate-data.aspx (accessed February 27, 2023).

[43] H. Li, J.J. Jiao, Analytical studies of groundwater-head fluctuation in a coastal confined aquifer overlain by a semi-permeable layer with storage, Adv. Water Resour. 24 (2001) 565–573, https://doi.org/10.1016/S0309-1708(00)00074-9.

[44] GEO, Dronninglund. Lunderbjerg 8A Damvarmelager - Vurdering af varmelagerets påvirkning af grundvand, 2012.

[45] A. Atangana, Principle of Groundwater Flow, in: Fract. Oper. With Constant Var. Order With Appl. to Geo-Hydrology, Elsevier, 2018, pp. 15–47, https://doi.org/10.1016/B978-0-12-809670-3.00002-3.

[46] J. Koch, J. Gotfredsen, R. Schneider, L. Troldborg, S. Stisen, H.J. Henriksen, High Resolution Water Table Modeling of the Shallow Groundwater Using a Knowledge-Guided Gradient Boosting Decision Tree Model, Front, Water. 3 (2021) 1–14, https://doi.org/10.3389/frwa.2021.701726.